Ab initio modeling of $CaTiO_3$ (110) polar surfaces

Jian-Min Zhang,[1] Jie Cui,[1] Ke-Wei Xu,[2] Vincent Ji,[3] and Zhen-Yong Man[4]
[1]*College of Physics and Information Technology, Shaanxi Normal University, Xi'an 710062, Shaanxi, People's Republic of China*
[2]*State Key Laboratory for Mechanical Behavior of Materials, Xi'an Jiaotong University, Xi'an 710049, Shaanxi, People's Republic of China*
[3]*ICMMO/LEMHE UMR CNRS 8182, Université Paris-Sud 11, 91405 Orsay Cedex, France*
[4]*State Key Laboratory of High Performance Ceramics and Superfine Microstructures, Shanghai Institute of Ceramics, Chinese Academy of Sciences, Shanghai 200050, People's Republic of China*
(Received 15 April 2007; revised manuscript received 21 June 2007; published 20 September 2007)

The TiO, Ca, asymmetric A-type O-terminated and symmetric B-type O-terminated surfaces have been constructed for $CaTiO_3$ (110) surface. The cleavage and surface energies, surface grand potential, surface relaxation, and surface electronic structure have been calculated for these polar terminations by using *ab initio* plane waves ultrasoft pseudopotential method based on generalized gradient approximation. The results show that the favorable $CaTiO_3$ (110) and (001) surfaces are CaO-terminated (001) surface, A-type O-terminated (110) surface, and TiO_2-terminated (001) surface successively, in view of the surface energy minimization. The Ca termination is stable in O- and Ca-rich environments, however, its complementary TiO termination is stable in O- and Ca-poor conditions. The A-type O termination shows a stability domain in moderate O and Ca environments. In the range of accessible values of $\Delta\mu_O$, only Ca and A-type O-terminated surfaces are likely to be observed. Moreover, a large surface rumpling s of 12.10% *a* is found for the TiO-terminated surface due to inward movement of Ti ion and outward movement of O ion. The surface band gaps for the relaxed TiO and A-type O terminations are larger than the bulk band gap; however, the values for Ca and B-type O terminations are smaller.

DOI: 10.1103/PhysRevB.76.115426 PACS number(s): 68.35.Bs, 68.35.Md, 68.47.Gh, 31.15.Ar

I. INTRODUCTION

Ferroelectric ABO_3 perovskite compounds constitute an important class of multifunctional materials and have been used extensively in various technological fields, such as high-capacity memory cells, catalysis, optical waveguides, integrated optics applications, and high-T_c cuprate superconductor growth.[1–10] The ferroelectricity in this class of compounds arises from a delicate balance between short-range forces favoring the undistorted cubic paraelectric structure, on the one hand, and long-range Coulomb interactions favoring a ferroelectric distortion, on the other hand.[5,6]

ABO_3 perovskite ferroelectric films are important for many applications. Compared with the bulk materials, the thin films have relatively larger surface and interface. Therefore, investigating how the physical properties are affected by the surface or interface is of primary importance. Recently, several *ab initio* theoretical studies were published for the surfaces of $BaTiO_3$ and $SrTiO_3$ crystals with fairly good agreement with experimental observations.[11–20]

$CaTiO_3$ is orthorhombic with space group *Pbnm* below 1380 K, and belongs to another orthorhombic space group *Cmcm* between 1380 and 1500 K. At 1500 K, it transforms into a tetragonal with space group 14/*mcm*. Above 1580 K, it becomes cubic with space group *Pm*-3*m*. Cubic $CaTiO_3$ is widely used in electronic ceramic materials and as a key component of synthetic rock used to immobilize nuclear waste.[21] Its critical transition temperature from the cubic phase to the low temperature phase of 1580 K is much higher than that of $BaTiO_3$ and $SrTiO_3$ (393 and 105 K, respectively), resulting in a different dielectricity and phase stability. The TiO_2-terminated (100) surface is energetically preferred over the BaO and SrO-terminated (100) surfaces for $BaTiO_3$ and $SrTiO_3$; however, the CaO-terminated (100) surface is preferred over the TiO_2-terminated (100) surface for $CaTiO_3$ since the Ca^{2+} is the smallest +2 cation in these titanates.[22]

Only the (100) surfaces of $CaTiO_3$ have been studied from theoretical views;[22,23] the (110) terminations are much less known, which is likely due to the polar character of the (110) orientation. The sequence of atomic layers of O_2 and CaTiO stoichiometry imply a monotonic raised microscopic electric field, which has to be compensated through either a modification of the surface composition or an anomalous filling of the surface electronic states. The former method will lead to nonstoichiometric terminations, while the latter implies crucial variations of the electronic structure of the surfaces that should be detected by experiments.

This paper is organized as follows. Some details of the calculation method and the structure of four different termination surfaces are given in Sec. II. The calculated cleavage and surface energies, surface grand potential, surface relaxation, and surface electronic structure of $CaTiO_3$ (110) surfaces are given in Sec. III. The conclusions of this work are summarized in Sec. IV.

II. METHOD

All calculations were performed within the framework of density functional theory using a basis set consisting of plane waves, as implemented in the Cambridge Serial Total Energy Package (CASTEP).[24] The electron-ion interactions were described by ultrasoft pseudopotentials, and electron exchange and correlation energies were calculated with the Perdew-

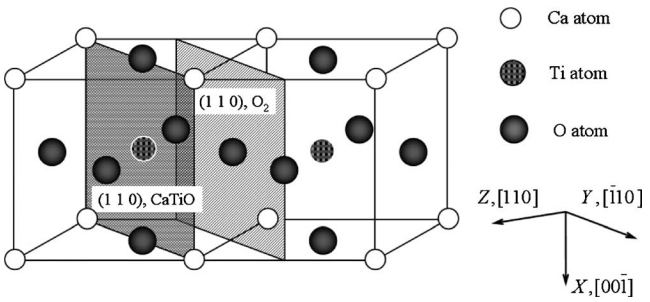

FIG. 1. Two terminations of the (110) surface: CaTiO and O_2.

Burke-Ernzerhof formulation of the generalized gradient approximation (GGA).[25] The structure was optimized with the Broyden-Fletcher-Goldfarb-Shanno method,[26] and the forces on each ion were converged to less than 0.01 eV/Å. The pseudopotentials used for bulk and slab were constructed by the electron configurations such as Ca $3s^2 3p^6 4s^2$ states, Ti $3s^2 3p^6 3d^2 4s^2$ states, and O $2s^2 2p^4$ states. The kinetic energy cutoff (400 eV) of the plane wave basis was used throughout, and the Brillouin zone was sampled with special k points of an $8\times8\times8$ grid for cubic structure and a $6\times5\times1$ grid for slab structure, respectively, as proposed by Monkhorst and Pack.[27] The energy tolerance was 5.0×10^{-6} eV/atom, the force tolerance was 0.01 eV/Å, and the displacement tolerance was 5.0×10^{-4} Å. The calculated values were obtained at 0 K.

Before the surface calculations, the bulk lattice constant a is calculated first, and the result of 3.874 Å is slightly smaller than the experimental value of 3.895 Å.[28] The theoretical lattice constant is used in following surface calculations.

Different from the (001) surface which consists of two types of neutral termination (CaO and TiO_2), the $CaTiO_3$ (110) surface (displayed in Fig. 1) consists of two charged planes (CaTiO and O_2). If the modeling slab consists of even number of (110) planes, that is, one termination is CaTiO with positive charge and the other is O_2 with negative charge, a nonzero macroscopic dipole moment perpendicular to the surface is obtained. If the modeling slab consists of odd number of (110) planes, that is, both terminations are identical CaTiO [Fig. 2(a)] or O_2 [Fig. 2(d)], a nonzero charged slab is obtained. The previous study showed that the two types of slab are unstable.[29]

To avoid this problem, as is shown in Fig. 2, viewed along the X direction in Fig. 1, we construct the other four modified polar slabs with neither dipole moment nor net charge. They are obtained by removing the Ca atoms from the CaTiO-terminated surface [Fig. 2(b)], the Ti and O atoms from the CaTiO-terminated surface [Fig. 2(c)], and half the O atoms from the O_2-terminated surface [Figs. 2(e) and 2(f)], respectively. If alternate columns of O atoms are removed from the O_2-terminated surface, as is shown in Fig. 2(e), the mirror symmetry about ($\bar{1}$10) plane (dashed line) will be broken and an asymmetric A-type configuration (missing column) is obtained. To maintain the symmetry, we move the remaining columns of the surface O atom along the [$\bar{1}$10] direction to

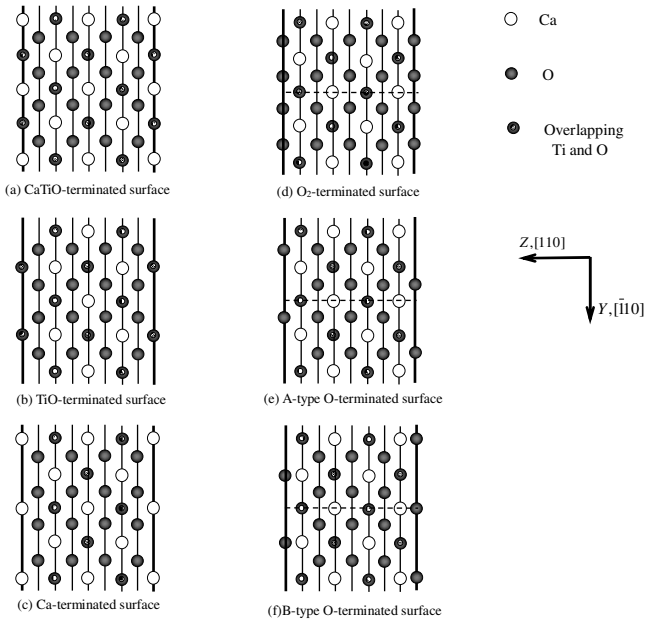

FIG. 2. Six initial atomic configurations of the $CaTiO_3$ (110) surface.

the middle of the distance between two equivalent O atoms in the bulk and a symmetric B-type configuration is obtained [Fig. 2(f)].

Four different (110) polar terminations of (1×1) supercell slab models and periodic boundary conditions are used in the repeated slab model calculations. For the considered four possible terminations, the slabs with nine atoms layer thickness are separated by a 12 Å vacuum region. During the surface structure optimization, all atoms are fully relaxed.

III. RESULTS AND DISCUSSIONS

A. Cleavage and surface energies

It is noted that the two nine layer TiO- and Ca-terminated (1×1) slabs represent together eight bulk unit cells, whereas the nine layer O-terminated (1×1) slab represents, by itself, four bulk unit cells. So we say that TiO- and Ca-terminated surfaces are complementary mutually, but each type of O-terminated surfaces is self-complementary.

The cleavage energy of the former $E_{cl}(\alpha)$ (α=TiO or Ca) can be obtained from the total energies computed for the unrelaxed slabs through the following equation:

$$E_{cl}(\alpha) = \frac{1}{4S}[E_{slab}^{unrel}(\mathrm{TiO}) + E_{slab}^{unrel}(\mathrm{Ca}) - nE_{bulk}], \qquad (1)$$

where E_{slab}^{unrel}(TiO) and E_{slab}^{unrel}(Ca) are the energies of unrelaxed TiO-terminated and Ca-terminated slabs, respectively. E_{bulk} is the bulk energy per formula unit in the cubic structure, n is the total number of bulk formula units in the two slabs, and 1/4 means that totally four surfaces are created upon the crystal cleavage.

When both sides of the slab are allowed to relax, the relaxation energies for each of the surfaces can be obtained by the equation

TABLE I. Calculated cleavage, relaxation, and surface energies of four different (110) terminations and two different (001) terminations of $CaTiO_3$, and the surface energies of $SrTiO_3$ and $BaTiO_3$ (110) and (001) surfaces are also listed for comparison. All values listed below are in J/m^2.

		(110)-terminated surfaces				(001)-terminated surfaces	
ATO_3	(A=Ca, Sr, Ba)	TiO	A	A-type O	B-type O	AO	TiO_2
$CaTiO_3$	E_{cl}	3.501	3.501	2.771	3.914	1.266	1.266
	E_{rel}	−1.321	−1.830	−1.933	−0.840	−0.442	−0.245
	E_{surf}	2.180	1.671	0.837	3.074	0.824	1.021
$SrTiO_3$[a]	E_{surf}	2.10 (HF)	2.97 (HF)	1.40 (HF)	3.08 (HF)	1.19 (LDA)	1.23 (LDA)
		2.21 (SM)	3.04 (SM)	1.54 (SM)	3.13 (SM)	1.18 (B3PW)	1.22 (B3PW)
$BaTiO_3$[b]	E_{surf}	2.04 (B3PW)	3.24 (B3PW)	1.72 (B3PW)		1.19 (B3PW)	1.07 (B3PW)
		2.35 (SM)	4.14 (SM)	1.81 (SM)		1.45 (SM)	1.40 (SM)

[a]References 14 and 15.
[b]References 16 and 17.

$$E_{rel}(\alpha) = \frac{1}{2S}[E_{slab}^{rel}(\alpha) - E_{slab}^{unrel}(\alpha)], \tag{2}$$

where $E_{slab}^{rel}(\alpha)$ (α=TiO or Ca) is the slab energy after the relaxation. Now when the cleavage and relaxation energies are calculated, the surface energy is just a sum of them,

$$E_{surf}(\alpha) = E_{cl}(\alpha) + E_{rel}(\alpha). \tag{3}$$

Since either A-type or B-type O-terminated surfaces are self-complementary, their cleavage energy E_{cl}(O), relaxation energy E_{rel}(O), and surface energy E_{surf}(O) can be calculated by the following equations:

$$E_{cl}(\mathrm{O}) = \frac{1}{2S}[E_{slab}^{unrel}(\mathrm{O}) - n' E_{bulk}], \tag{4}$$

$$E_{rel}(\mathrm{O}) = \frac{1}{2S}[E_{slab}^{rel}(\mathrm{O}) - E_{slab}^{unrel}(\mathrm{O})], \tag{5}$$

$$E_{surf}(\mathrm{O}) = E_{cl}(\mathrm{O}) + E_{rel}(\mathrm{O}) = \frac{1}{2S}[E_{slab}^{rel}(\mathrm{O}) - n' E_{bulk}], \tag{6}$$

where n' is the total number of bulk formula units in each slab, and E_{slab}^{rel}(O) and E_{slab}^{unrel}(O) are the energies of the O-terminated slab with and without relaxation, respectively.

Our *ab initio* calculated results of the cleavage, relaxation, and surface energies of the four different (110) terminations are listed in Table I. It is noted that the A-type O termination corresponds to the lowest cleavage and surface energies (2.771 and 0.837 J/m^2) among the four terminations, whereas the B-type O termination possesses of the highest ones (3.914 and 3.074 J/m^2). It can be predicted by the values of surface energies that the favorable (110) surfaces of $CaTiO_3$ are A-type O-, Ca-, and TiO-terminated surfaces and B-type O-terminated surface successively. In order to compare with the (001) surface, the cleavage, relaxation, and surface energies have also been calculated for CaO- and TiO_2-terminated (001) surfaces, and the results are also listed in Table I. From surface energy minimization, we can conclude that in $CaTiO_3$ (001) and (110) surfaces, the three favorable surfaces are the CaO-terminated (001) surface, A-type O-terminated (110) surface, and TiO_2-terminated (001) surface successively.

The surface energies calculated by Heifets *et al.*[14–17] for $SrTiO_3$ and $BaTiO_3$ (110) and (001) surfaces are also listed in Table I. We can see that the A-type O-terminated (110) surface is the most stable for $SrTiO_3$ and $BaTiO_3$ (110) surfaces, in line with the present study for $CaTO_3$ (110) surface. For $SrTiO_3$ and $BaTiO_3$, however, the surface energies of the two types of (001) surfaces are consistently lower than those of the A-type O-terminated surfaces, which is different from our result that the surface energy of the A-type O-terminated (110) surface is a little higher than that of the TiO_2-terminated (001) surface for $CaTiO_3$.

B. Surface grand potential

Although the values of E_{surf} are used generally as an indication of the stability of the split crystal in vacuum, they give no information about which termination is the most stable in practical environment conditions. In experiments, for example, one of the standard control parameters is the oxygen pressure in the vacuum chamber. In order to compare the relative stability, the surface grand potential, which implies a contact with matter reservoirs, has been calculated for four constructed terminations with the equation[30,31]

$$\Omega(\alpha) = \frac{1}{2S}[E_{slab}^{rel}(\alpha) + PV - TS - n_{\mathrm{Ca}}\mu_{\mathrm{Ca}} - n_{\mathrm{Ti}}\mu_{\mathrm{Ti}} - n_{\mathrm{O}}\mu_{\mathrm{O}}], \tag{7}$$

where $\Omega(\alpha)$ (α=TiO, Ca, or O) is the surface grand potential per unit area of α termination, the μ_{Ca}, μ_{Ti}, and μ_{O} are the chemical potentials of the Ca, Ti, and O atomic species, and n_{Ca}, n_{Ti}, and n_{O} are the number of Ca, Ti, and O atoms in the slab, respectively. For typical pressure P and temperature T, the PV and $-TS$ terms can be neglected with respect to other contributions. Since $CaTiO_3$ is a ternary oxide, the chemical potential $\mu_{\mathrm{CaTiO_3}}$ of the cubic phase is written as a sum of three terms representing the chemical potential of each species within the crystal:

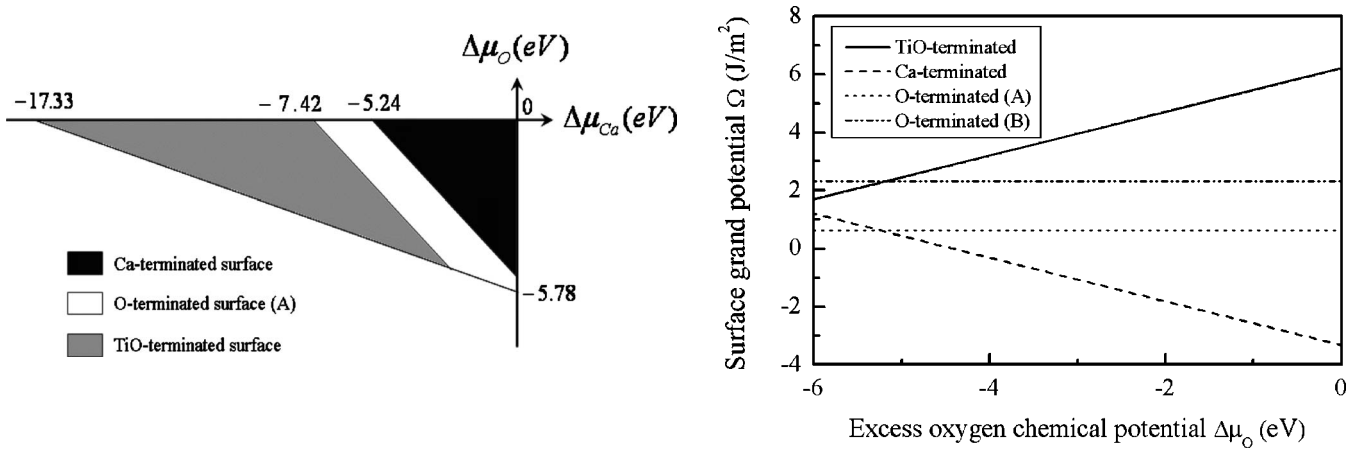

FIG. 3. Stability diagram of the $CaTiO_3$ (110) surface. The most stable termination is represented on the left as a function of the excess O and Ca chemical potentials $\Delta\mu_O$ and $\Delta\mu_{Ca}$. On the right, the surface grand potentials are represented as a function of $\Delta\mu_O$ (for a particular value of the Ca chemical potential $\Delta\mu_{Ca}=0$ eV).

$$\mu_{CaTiO_3} = \mu_{Ca} + \mu_{Ti} + 3\mu_O. \tag{8}$$

As long as the surface is in equilibrium with the bulk $CaTiO_3$, we have $\mu_{CaTiO_3}=E_{bulk}$. Substituting Eq. (8) into Eq. (7), we can eliminate the μ_{Ti} variable in the surface grand potential:

$$\Omega(\alpha) = \frac{1}{2S}[E^{rel}_{slab}(\alpha) - n_{Ti}E_{bulk} - \mu_O(n_O - 3n_{Ti}) - \mu_{Ca}(n_{Ca} - n_{Ti})]. \tag{9}$$

If the minimum and maximum values of the O and Ca chemical potentials are known, we can deduce the range of the accessible values of $\Omega(\alpha)$ for each termination according to Eq. (9).

Introducing the variations of the chemical potentials with respect to the reference phases ($\Delta\mu_O=\mu_O-E^{mol}_{O_2}/2$ and $\Delta\mu_{Ca}=\mu_{Ca}-E^{bulk}_{Ca}$), we can obtain from Eq. (9) the following:

$$\Omega(\alpha) = \phi(\alpha) - \frac{1}{2S}[\Delta\mu_O(n_O - 3n_{Ti}) - \Delta\mu_{Ca}(n_{Ca} - n_{Ti})], \tag{10}$$

$$\phi(\alpha) = \frac{1}{2S}\left[E^{rel}_{slab}(\alpha) - n_{Ti}E_{bulk} - \frac{1}{2}E^{mol}_{O_2}(n_O - 3n_{Ti}) - E^{bulk}_{Ca}(n_{Ca} - n_{Ti})\right]. \tag{11}$$

$\phi(\alpha)$ expresses the stability of the surface with respect to bulk $CaTiO_3$, molecular oxygen, and metallic Ca, while (n_O-3n_{Ti}) represents the excess (if positive) or the deficiency (if negative) in the number of oxygen atoms of the terminations.

In order to estimate the surface grand potential $\Omega(\alpha)$, we plot the stability diagram of $CaTiO_3$ (110) surfaces in an O and Ca external environment and we also plot $\Omega(\alpha)$ as a function of $\Delta\mu_O=\mu_O-E^{mol}_{O_2}/2$. Small values of $\Delta\mu_O$ and $\Delta\mu_{Ca}$ correspond to O-poor and Ca-poor conditions, while large values are associated with high oxygen and high calcium conditions, respectively.

First of all, according to Fig. 3 (left panel), our calculations predict that only three out of the four possible terminations can be formed. Indeed, the B-type O termination cannot be stabilized, even in very O-rich chemical environment. The Ca termination is the most stable one in O- and Ca-rich environments, however, its complementary TiO termination is stable in O- and Ca-poor conditions. The A-type O termination shows a stability domain in moderate O and Ca environments. In the right figure, the surface grand potentials are represented as a function of $\Delta\mu_O$ (for a particular value of the Ca chemical potential $\Delta\mu_{Ca}=0$ eV). We can see that in the range of accessible values of $\Delta\mu_O$, only the Ca termination and the A-type O termination are likely to be observed. Furthermore, the Ca termination is the dominant of the two likely terminations in the range of accessible values of $\Delta\mu_O$.

C. Surface relaxation

The relaxed structures of the four different terminations of the $CaTiO_3$ (110) surface have been calculated by allowing all nine layers to relax fully until the minimum of the system's energy is reached. The results are presented in Table II. The displacements of the ion on the ith layer from the surface are expressed as Δy_i and Δz_i:

$$\Delta y_i = (y_i - y_{i,bulk})/a \times 100\,\%\,, \tag{12}$$

$$\Delta z_i = (z_i - z_{i,bulk})/a \times 100\,\%\,. \tag{13}$$

Here, y_i and z_i are the y and z coordinates of Ca, Ti, and/or O in the ith layer after relaxation, and $y_{i,bulk}$ and $z_{i,bluk}$ are the unrelaxed y and z coordinates determined from the theoretical lattice constant a of cubic $CaTiO_3$. $\Delta z_i<0$ indicates the direction inward the surface; on the contrary, $\Delta z_i>0$ means the direction outward the surface. The amplitudes of the surface rumpling s (the relative displacement of oxygen with respect to the metal atom in the surface layer) and the changes in interlayer distances between the first and second

TABLE II. Relaxation of the uppermost four layers in the TiO-, Ca-, and O-terminated $CaTiO_3$ (110) surfaces (as a percentage of the bulk crystal lattice parameter a=3.874 Å).

TiO terminated			Ca terminated			O terminated				
								A		B
Layer	Ion	Δz (%)	Layer	Ion	Δz (%)	Layer	Ion	Δy (%)	Δz (%)	Δz (%)
1	Ti	−4.95	1	Ca	−15.37	1	O	−7.90	−11.54	−7.03
	O	7.15	2	O	2.52	2	Ca	−2.37	1.07	6.61
2	O	−0.90	3	Ca	−3.29		Ti	−4.53	0.44	−2.12
3	Ca	−3.09		Ti	0.89		O	8.06	6.35	5.99
	Ti	0.28		O	−2.15	3	O	−10.94	−6.78	−0.84
	O	−4.04	4	O	0.35	4	Ca	−2.68	−5.29	−2.73
4	O	0.19					Ti	−0.01	1.63	0.46
							O	1.72	−0.27	−1.08

crystal layers (Δd_{12}) and between the second and third crystal layers (Δd_{23}) are presented in Table III.

On the TiO-terminated surface, Ti ions on the first layer move 4.95% a inward, whereas O ions move 7.15% a outward, which lead to a large surface rumpling s of 12.10% a. This relaxation is larger than that of the (100) surface calculated by Wang *et al.*,[20] and the reduction of relative distances between the first three layers is 5.23% a. On Ca-terminated surface, Ca ions on the first layer move inward by 15.37% a and the reduction of relative distances between the first three layers (11.22% a) is much larger than that of the TiO-terminated surface. The O ions on the first layer of the A-type O-terminated surface move not only 11.54% a inward but also 7.90% a along the negative direction of the y axis due to asymmetry. On the second layer, Ca ions move 2.37% a in the negative y direction and 1.07% a outward the slab. Ti ions move 4.53% a along the negative y direction and only 0.44% a outward. O ions move by 6.35% a and 8.06% a in the directions opposite to those on the first layer. The displacements of the O ions on the third layer are still large. The larger ionic displacements result in large Δd_{12} and Δd_{23} (−11.98% a and 7.72% a, respectively). All ions on the B-type O-terminated surface move only perpendicular to the surface, as expected by the symmetry. The O ions on the first layer and Ti ions on the second layer move by 7.03% a and 2.12% a inward, whereas the second-layer Ca and O ions move outward by 6.61% a and 5.99% a. The displacements of the O ions on the third layer are very small.

TABLE III. Surface rumpling s and relative displacements of the three near-surface layers for the TiO-, Ca-, and O-terminated $CaTiO_3$ (110) surfaces (as a percentage of the bulk crystal lattice parameter).

Termination	s	Δd_{12}	Δd_{23}
TiO terminated	12.10	−4.05	−1.18
Ca terminated		−12.85	1.63
A-type O terminated		−11.98	7.22
B-type O terminated		−4.91	−1.28

D. Surface electronic structure

We calculated the electronic structure for both bulk and four terminated surfaces, and the density of states (DOS) for the Ca, TiO, and O (two types) terminations around the Fermi level are shown in Fig. 4. The calculated bulk band gap of 1.877 eV is smaller than the experimental value of 3.5 eV, which is caused by the GGA calculations. The surface band gaps for the relaxed TiO and A-type O termina-

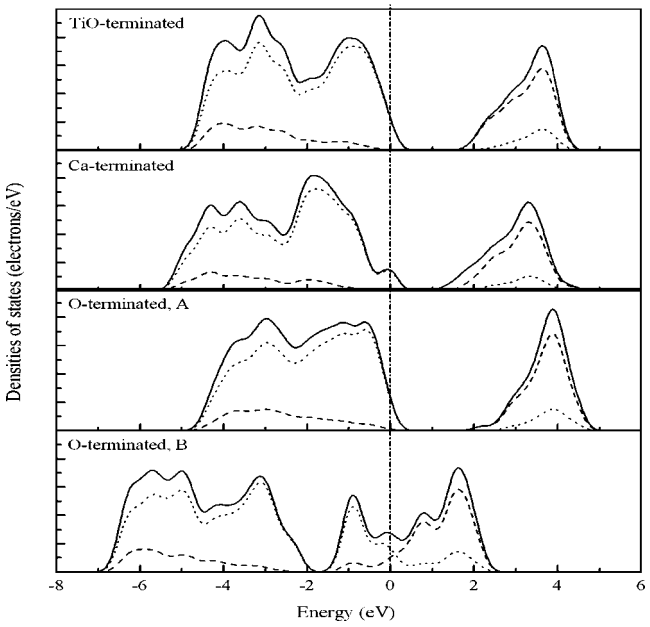

FIG. 4. Density of states for the TiO, Ca, and O (two types) terminations around the Fermi level. Solid line, total density of states; dotted line, p partial density of states; and dashed line, d partial density of states. The Fermi level is indicated by the dash dotted line.

tions are 1.885 and 2.000 eV, slightly larger than the bulk band gap; however, for Ca and B-type O terminations, the values reduced to 1.173 and 1.042 eV, respectively. We can see that the DOS of B-type O termination is much different from the other three terminations such that the conduction bands are introduced into the bulk band gap.

IV. CONCLUSIONS

In the present work, the TiO, Ca, asymmetric A-type O-terminated and symmetric B-type O-terminated surfaces have been constructed for the $CaTiO_3$ (110) surface. The cleavage and surface energies, surface grand potential, surface relaxation, and surface electronic structure have been calculated for these polar terminations by using *ab initio* plane waves ultrasoft pseudopotential method based on GGA. The following conclusions are obtained:

(1) In $CaTiO_3$ (001) and (110) surfaces, the three favorable surfaces are the CaO-terminated (001) surface, A-type O-terminated (110) surface, and TiO_2-terminated (001) surface successively.

(2) The Ca termination is stable in O- and Ca-rich environments, however, its complementary TiO termination is stable in O- and Ca-poor conditions. The A-type O termination shows a stability domain in moderate O and Ca environments.

(3) In the range of accessible values of $\Delta\mu_O$, only the Ca termination and the A-type O termination are likely to be observed, especially the former.

(4) A large surface rumpling s of 12.10% a is found for the TiO-terminated surface, caused by the movement inward of the Ti ion and the movement outward of the O ion.

(5) The surface band gaps for the relaxed TiO and A-type O terminations are larger than the bulk band gap, however, the values for Ca and B-type O terminations are smaller.

ACKNOWLEDGMENTS

The authors would like to acknowledge the State Key Development for Basic Research of China (Grant No. 2004CB619302) and the National Natural Science Foundation of China (Grant No. 50271038) for providing financial support for this research.

[1] I. A. Kornev, L. Bellaiche, P. Bouvier, P.-E. Janolin, B. Dkhil, and J. Kreisel, Phys. Rev. Lett. **95**, 196804 (2005).
[2] I. I. Naumov, L. Bellaiche, and H. X. Fu, Nature (London) **432**, 737 (2004).
[3] J. H. Haeni, P. Irvin, W. Chang, R. Uecker, P. Reiche, Y. L. Li, S. Choudhury, W. Tian, M. E. Hawley, B. Craigo, A. K. Tagantsev, X. Q. Pan, S. K. Streiffer, L. Q. Chen, S. W. Kirchoefer, J. Levy, and D. G. Schlom, Nature (London) **430**, 758 (2004).
[4] J. Junquera and Ph. Ghosez, Nature (London) **422**, 506 (2003).
[5] R. E. Cohen and H. Krakauer, Phys. Rev. B **42**, 6416 (1990).
[6] R. Cohen, Nature (London) **358**, 136 (1992).
[7] C. Noguera, *Physics and Chemistry at Oxide Surfaces* (Cambridge University Press, New York, 1996).
[8] M. E. Lines and A. M. Glass, *Principles and Applications of Ferroelectrics and Related Materials* (Clarendon, Oxford, 1977).
[9] O. Auciello, J. F. Scott, and R. Ramesh, Phys. Today **51** (7), 22 (1998).
[10] Proceedings of the Williamsburg Workshop on Fundamental Physics of Ferroelectrics-99 [J. Phys. Chem. Solids **61**, 139 (2000)].
[11] A. Asthagiri and D. S. Sholl, J. Chem. Phys. **116**, 9914 (2002).
[12] A. Asthagiri and D. S. Sholl, Surf. Sci. **581**, 66 (2005).
[13] A. Asthagiri, C. Niederberger, A. J. Francis, L. M. Porter, P. A. Salvador, and D. S. Sholl, Surf. Sci. **537**, 134 (2003).
[14] E. Heifets, W. A. Goddard III, E. A. Kotomin, R. I. Eglitis, and G. Borstel, Phys. Rev. B **69**, 035408 (2004).
[15] E. Heifets, R. I. Eglitis, E. A. Kotomin, J. Maier, and G. Borstel, Phys. Rev. B **64**, 235417 (2001).
[16] R. I. Eglitis, G. Borstel, E. Heifets, S. Piskunov, and E. Kotomin, J. Electroceram. **16**, 289 (2006).
[17] E. Heifets, E. Kotomin, and J. Maier, Surf. Sci. **462**, 19 (2000).
[18] C. Cheng, K. Kunc, and M. H. Lee, Phys. Rev. B **62**, 10409 (2000).
[19] L. Fu, E. Yaschenko, L. Resca, and R. Resta, Phys. Rev. B **60**, 2697 (1999).
[20] F. Cora and C. R. A. Catlow, Faraday Discuss. **114**, 421 (1999).
[21] A. E. Ringwood, S. E. Kesson, K. D. Reeve, D. M. Levins, and E. J. Ramm, *Radioactive Waste Forms for the Future* (Elsevier, Amsterdam, 1988).
[22] S. P. Chen, J. Mater. Res. **13**, 1848 (1998).
[23] Y. X. Wang, M. Arai, T. Sasaki, and C. L. Wang, Phys. Rev. B **73**, 035411 (2006).
[24] M. D. Segall, P. L. D. Lindan, M. J. Probert, C. J. Pickard, P. J. Hasnip, S. J. Clark, and M. C. Payne, J. Phys.: Condens. Matter **14**, 2717 (2002).
[25] J. P. Perdew, K. Burke, and M. Ernzerhof, Phys. Rev. Lett. **77**, 3865 (1996).
[26] T. H. Fischer and J. Almlof, J. Phys. Chem. **96**, 9768 (1992).
[27] H. J. Monkhorst and J. D. Pack, Phys. Rev. B **13**, 5118 (1976).
[28] B. J. Kennedy, C. J. Howard, and B. Chakoumakos, J. Phys.: Condens. Matter **11**, 1479 (1999).
[29] P. W. Tasker, J. Phys. C **12**, 4977 (1979).
[30] X. G. Wang, A. Chaka, and M. Scheffler, Phys. Rev. Lett. **84**, 3650 (2000).
[31] A. Pojani, F. Finocchi, and C. Noguera, Surf. Sci. **442**, 179 (1999).